Numerical Simulation Flow Around the Containership by using CFD Method

Nguyen Thi Ngoc Hoa[1,*], Tat-Hien Le[2,3], Le Doan Nhat Huy[2,3]

[1] Ho Chi Minh City University of Transport, Vietnam
[2] Ho Chi Minh City University of Technology (HCMUT), Vietnam
[3] Vietnam National University Ho Chi Minh City, Vietnam

ARTICLE INFO	ABSTRACT
	Predict accurately resistance of the ship and flow around ship hull form is extremely important as these are input parameters for optimizing ship hull form, designing the ship propulsion system. This paper focuses on the numerical simulation of the flow around the Container Ship Fortune Freighter in calm water condition at different ship speeds by using CFD method. The results of impact of ship speed on components of ship resistance, wave patterns, volume fraction of air, the distribution of pressure, and wall shear stress on the ship's hull surface, as well as the nominal wake field are provided and analysed in this paper.

1. Introduction

In the design of ship hull forms, predicting accurately resistance of the ship and flow around ship hull form is extremely crucial as these are input parameters for various aspects, including the optimization of the ship hull form to minimize ship resistance, and correct the design of the ship's propulsion system effectively.

Nowadays, researchers all over the world tend to use two methods to predict ship resistance and obtain information on the flow field around the ship, including the experimental and the Computational Fluid Dynamics (CFD) methods. The first method offers the most dependable data regarding the ship resistance and flow around the ship hull. Nonetheless, this method entails high costs and is time-consuming. A more favorable alternative, the CFD method can provide relatively accurate results and furnish more intricate details of the flow around the ship hull with a shorter time and at a lower cost compared to the experimental method [1]. Consequently, the CFD method has been universally adopted for investigating the ship resistance and flow around the hull [2-13].

Hänninen and Sehweighofer [10] investigated the flow around the containership Hamburg Test Case at different scales using the CFD method. The results of this research have provided the different

flow fields around the hull at various model scales. Hoa [14] and Tu *et al.,* [15] assessed the influence of the selected turbulent model on the flow characteristics around the DTMB 5415 ship in model scale. Their research proved that the chosen turbulence model significantly impacts not only the numerical results in resistance but also the characteristics of flow around the ship. Ahmed *et al.,* [9] used both CFD and experimental methods for validating the resistance of DTMB vessel. Hoa [14] applied CFD method to discover the influence of water depth on ship resistance. Using the same method, Le *et al.,* [16] studied the effect of trim on a DTMB vessel at different drafts and ship speeds, revealing the similar results and concluded that the optimal trim varies significantly with ship speeds and drafts. These reviewed studies provide valuable references for using the CFD method in predicting the ship resistance and simulating the flow fields around the hull. This paper focuses on the investigation of the resistance and flow around the containership Fortune Freighter at different ship speeds in calm water condition using the CFD appliance.

2. Methodology
2.1 Reynolds-Averaged Navier-Stokes Equations

The application of time-averaging to the momentum and continuity equations for Reynolds Averaged Navier-Stokes equation (RANSE) is written as [4]

$$\frac{\partial(\rho \bar{u}_i)}{\partial x_i} = 0 \tag{1}$$

and

$$V_j \frac{\partial V_i}{\partial x_j} = -\frac{1}{\rho}\frac{\partial P}{\partial x} + \frac{\partial}{\partial x_j}\left[\left(\frac{\partial V_i}{\partial x_j} + \frac{\partial V_j}{\partial x_i}\right)\right] + \frac{1}{\rho}\frac{\partial \tau_{ij}}{\partial x_j} \tag{2}$$

where: ρ is the fluid density, x_i and x_j are the coordinates, v presents the fluid kinematic viscosity, τ_{ij} is the Reynolds stresses tensor; P and V_i are the time-averaged pressure and velocity components, respectively.

2.2 SST K-ω (SSTKO) Turbulence Models

SST K-ω turbulence model are two variants of k-omega turbulence models that solve transport equations for k and ω to calculate μ_t. And μ_t is defined by the below equation [15]

$$\mu_t = \rho k T \tag{3}$$

The turbulent time scale (T) is defined as follows

$$T = \min\left(\frac{a^*}{\omega}, \frac{a_1}{SF_2}\right) \tag{4}$$

The *k* and ω are estimated as follows

$$\frac{\partial}{\partial t}(\rho k)+\nabla\cdot(\rho k\overline{v})=\nabla\cdot\left[\left(\mu+\sigma_k\mu_t\right)\nabla k\right]+P_k-\rho\beta*f_{\beta*}(k\omega-k_0\omega_0)+S_k \tag{5}$$

$$\frac{\partial}{\partial t}(\rho\omega)+\nabla\cdot(\rho\omega\overline{v})=\nabla\cdot\left[\left(\mu+\sigma_\omega\mu_t\right)\nabla\omega\right]+P_\omega-\rho\beta f_\beta(\omega^2-\omega_0^2)+S_\omega \tag{6}$$

where a^*, a_1 represent the model coefficients, f_β and $f_{\beta*}$ present the vortex-stretching and free-shear modification factors, F_2 is a blending function, P_k and P_ω represent production terms, S_ω are user-specified source terms, σ_ω is a model coefficient.

The coefficients in equations from (3) to (6) are selected following the recommendations of user guide of Star-CCM+ [17].

3. Numerical Setup
3.1 Reference Vessel

The container ship Fortune Freighter is selected to be the reference vessel. The principal parameters and geometry of this ship are depicted in Table 1 and Figure 1 [18].

Table 1
Principal particulars of containership Fortune Freighter [18]

Parameters	Symbol	Unit	Value
Ship length between perpendiculars	L_{PP}	[m]	113.60
Ship breadth	B	[m]	18.50
Ship design draught	T	[m]	8.00
Displacement	Δ	[tone]	12763
Block coefficient	C_B	[-]	0.738
Wetted surface area	S	[m^2]	3214
Container capacity	n_{TEU}	[TEU]	566
Main engine power	Ps	[kW]	5960

Fig. 1. The containership Fortune Freighter

3.2 Case Study

This study applied a commercial CFD code Star-CCM+ (Version 16.02 2021.1) to perform the numerical computations. The simulation was configured with the following settings
  i.   Calm water condition;
  ii. The vessel is free to trim and sink;
  iii. The displacement of the ship is constant for different ship speeds;
  iv. The hull roughness $k_S = 150 \times 10^{-6}$ m;
  v.   The water parameters for all case studies (density, viscosity) were taken corresponding to the realistic seawater properties at temperature 23^0 (water density $\rho = 1024.16$ kg/m^3, kinematic viscosity of water $v = 1.00836 \times 10^{-6}$ m^2/s).

3.3 Computational Domain and Boundary Condition

To enhance the ship resistance computation efficiency, only half of the ship hull was modelled as the ship hull is symmetry along its longitudinal plane. The computational domain size was defined following the guidelines of the ITTC (International Towing Tank Conference) [19]. Consequently, the inlet and outlet boundaries were established at distances of 1.5L_{PP} and 2.5L_{PP} from the bow and stern of the ship, respectively. The top, bottom, and side boundaries were positioned at distances of 1.5L_{PP}, 2.5L_{PP}, and 2.5L_{PP} from the ship, respectively (see Figure 2).
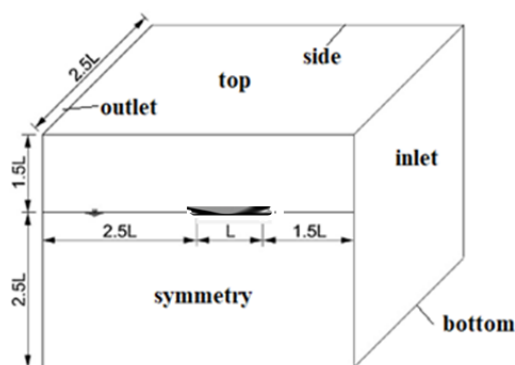
Fig. 2. The Computational domain size

The chosen boundary conditions are as follows: within the computational domain, constant velocity is set for the inlet, bottom, and top boundaries; the outlet boundary is subject to hydrostatic pressure; symmetry plane is applied to the side and symmetry plane boundaries, for the ship hull, a no-slip wall condition is employed.

3.4 Mesh Generation and Physical Model

The mesh is a critical factor that significantly influences the accuracy of the numerical obtained results. In this study, a combination of trimmed mesh and prism layer meshes were employed for meshing purposes. The computational domain was discretized into finite volumes using a trimmed mesh. Refinement of the mesh was carried out in the vicinity of the ship hull and the free surface to acquire the exact flow near the hull and at the free surface. To prevent unnecessary use of fine grid resolution where not essential, local volume refinement was only implemented at ship bow and ship stern. Prism layer meshes were incorporated to accurately capture the exact boundary layer between walls and flow. Figure 3 illustrates the result of the mesh generation process.
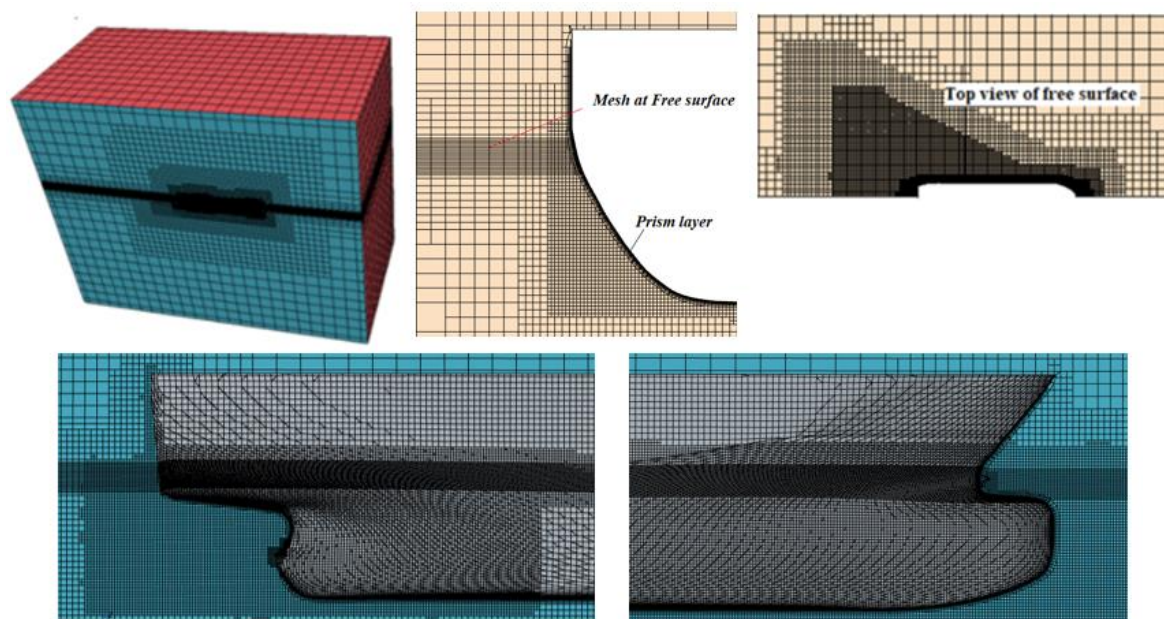
Fig. 3. The result of mesh generation

The physical model used in this research is the unsteady RANSE method with the SST (Shear Stress Transport) K-Omega turbulence model. This model proved to predict ship hydrodynamics accurately [15]. The VOF (Volume of Fluid) technique was applied to model the free surface. The two degrees of freedom motion is employed to allow ship motion in heave and pitch direction. DFBI (Dynamic Fluid Body Interaction) Equilibrium option is used to simulate the motion of the hull during the computation [13,16].

4. Results and Discussion
4.1 Numerical Results of Ship Resistance and Ship Motion

Table 2, Figure 4 and Figure 5 show the numerical results of ship resistance and the ship motion at design draught T=8.00m for different ship speeds (Vs) in calm water condition. In Table 2, the symbols RT, RF, and RP represent the total ship resistance, frictional resistance, and pressure resistance components, respectively. Some conclusions can be produced from the results depicted in Table 2, as follows

  i. When the ship operates at different speeds, the ship's resistance and motions change.
 ii. The frictional and pressure resistance components have the same monotonically changing trend at different ship speeds, but different in the magnitude of changing. Specifically, a larger increase is observed in the pressure resistance than in frictional resistance with increasing the ship speed. As a result, the ratio of frictional resistance and pressure resistance reduces with increasing the ship speed. This trend is perfectly consistent with the literature mentioned in documents [1,20]. This can be explained by the difference in the flow field around the ship hull presented in Section 3.2 of this paper.
iii. Trim and sinkage of the ship increase monotonically with increasing ship speed.

Table 2
The numerical results of ship resistance and ship motion at different ship speeds in calm water condition

Vs [knots]	Ship resistance components				Ship motion	
	R_T [kN]	R_F [kN]	R_P [kN]	R_F/R_P	Trim (deg.)	Sinkage (m)
11.0	148.20	111.60	36.60	3.05	0.112	-0.122
13.0	229.60	157.20	72.40	2.17	0.161	-0.179
15.0	329.50	207.40	122.10	1.70	0.214	-0.239
17.0	475.40	261.00	214.40	1.22	0.308	-0.333
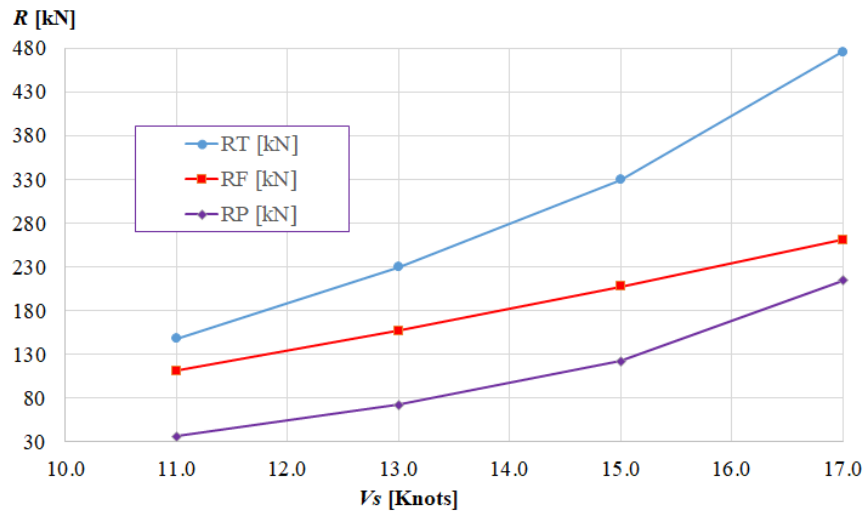
Fig. 4. The relationship between the ship resistance components versus ship speeds
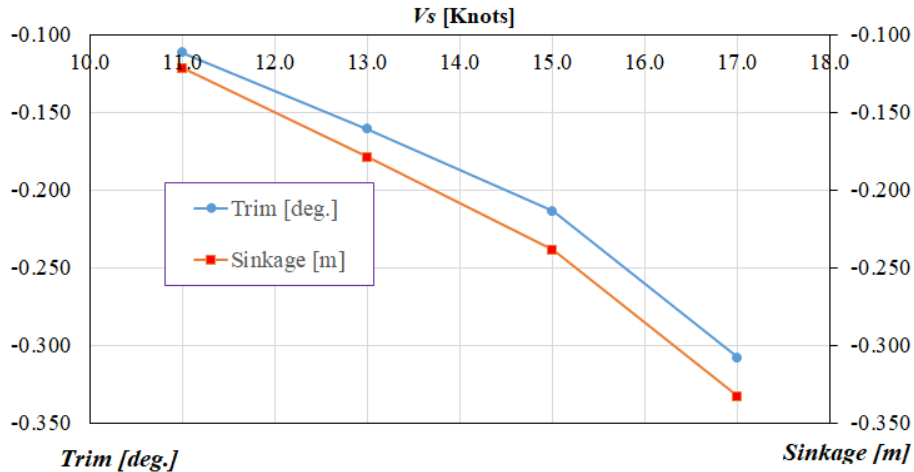
Fig. 5. The relationship between the ship motion versus ship speeds

4.2 Flow Around the Ship

The features of the flow around the containership hull are presented in Figure 6 to Figure 13. This could not only explain the change of ship resistance versus the ship speed, but also is an important input data for the hull shape optimization in terms of minimizing ship resistance. As can be seen in Figure 6 and Figure 7 that, the wave amplitude on the free surface exhibits a monotonic increase with increasing of ship speed. The wave amplitude reaches the biggest value at Vs=17.0 knots, while the smallest one occurs at Vs=11.0 knots. This variation in wave amplitude partially causes the increase in the pressure resistance component.
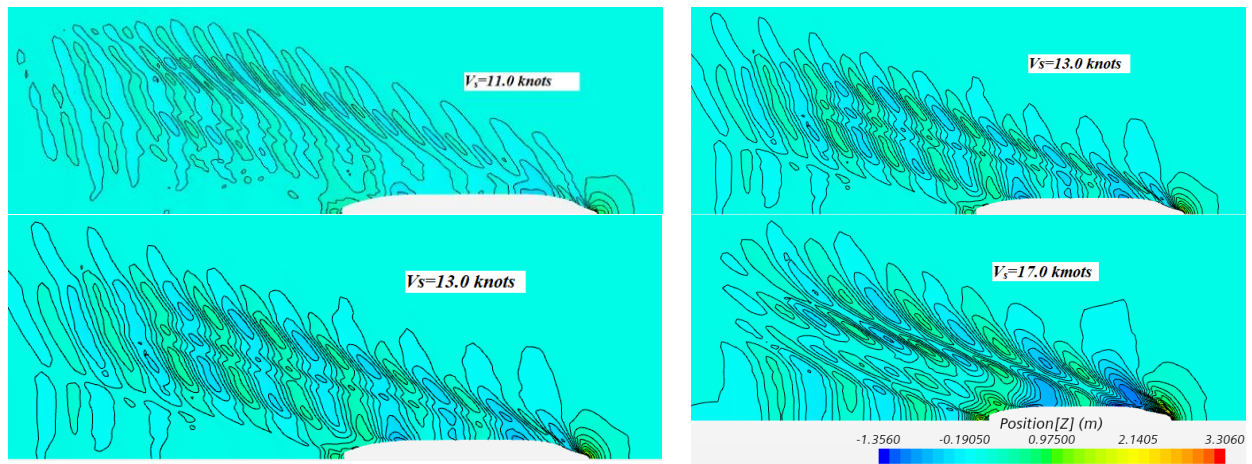
Fig. 6. Wave pattern at various ship speeds
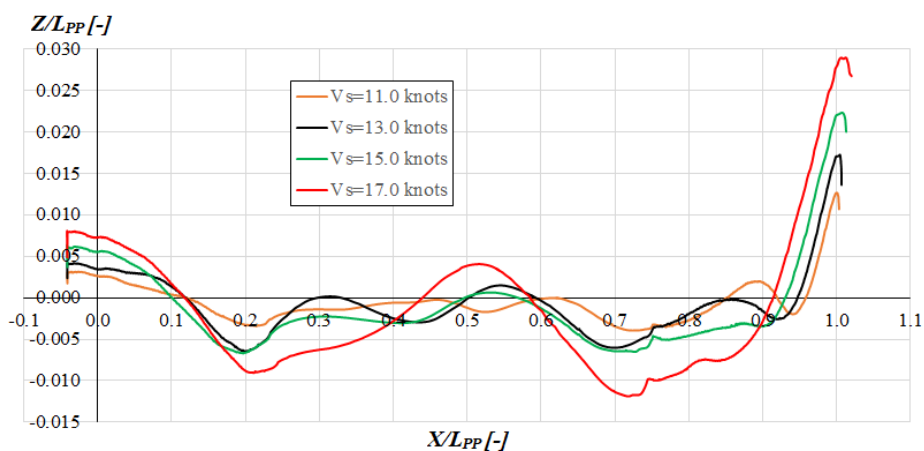
Fig. 7. Wave's profile along the ship hull at various ship speeds

Figure 8 illustrates the variation in air volume fraction across different parts of the ship at different ship speeds. As evident from the figure, at the bow of the containership, the volume fraction of air rises gradually when ship speed increases.
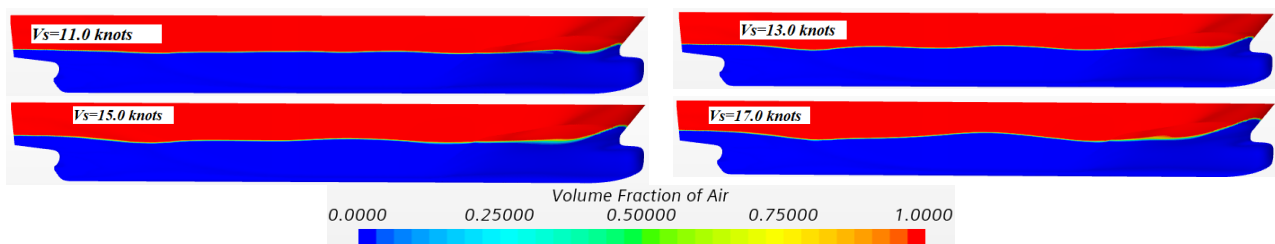
Fig. 8. Volume fraction of air at various ship speeds

Figure 9 and Figure 10 show the variations in the dynamic pressure coefficient distribution on the containership hull surface at different ship speeds. These visualizations offer valuable insights into the observed changes in the pressure resistance component at varying speeds. As evident from Figure 9 and Figure 10, across the location from stern of the ship to X/L = 0.2 and from X/L=1.0 to ship's bow, the dynamic pressure coefficient is almost the same at various of ship speeds. Conversely, the region between X/L = 0.2 and X/L= 1.0 presents differences in the pressure coefficient at various ship speeds.
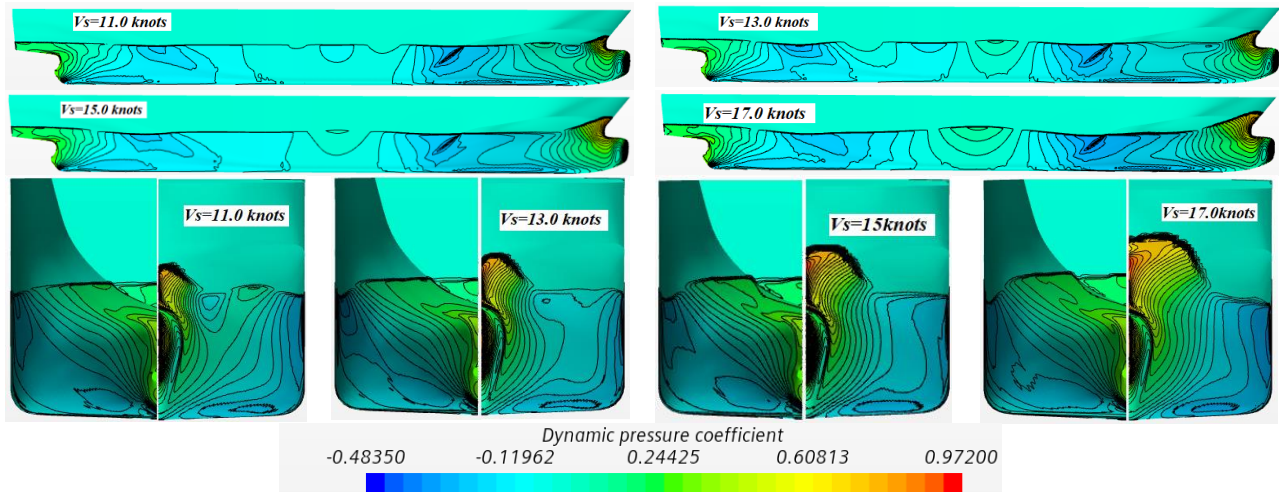
Fig. 9. Dynamic pressure coefficient distribution on the containership hull surface at various ship speeds
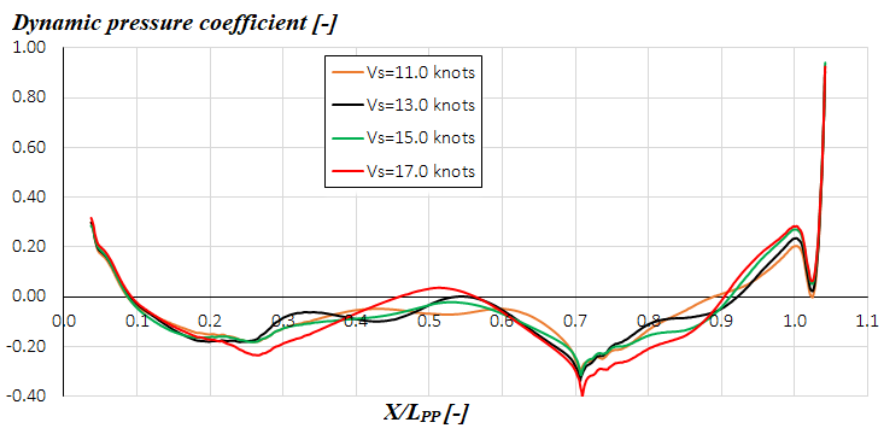
Fig. 10. Dynamic pressure coefficient at Z =4m with different ship speeds

The variations in wall shear stress distribution contribute to explaining the changes observed in the friction resistance component at various ship speeds. Figure 11 and Figure 12 depict the discrepancy in wall shear stress distribution on the hull surface at various ship speeds. It can be observed in Figure 12 that, the wall shear stress at Z=4.0m changes monotonically with various ship speeds. The highest and smallest wall shear stress values are observed at Vs=17.0 knots and Vs=11.0 knots, respectively.
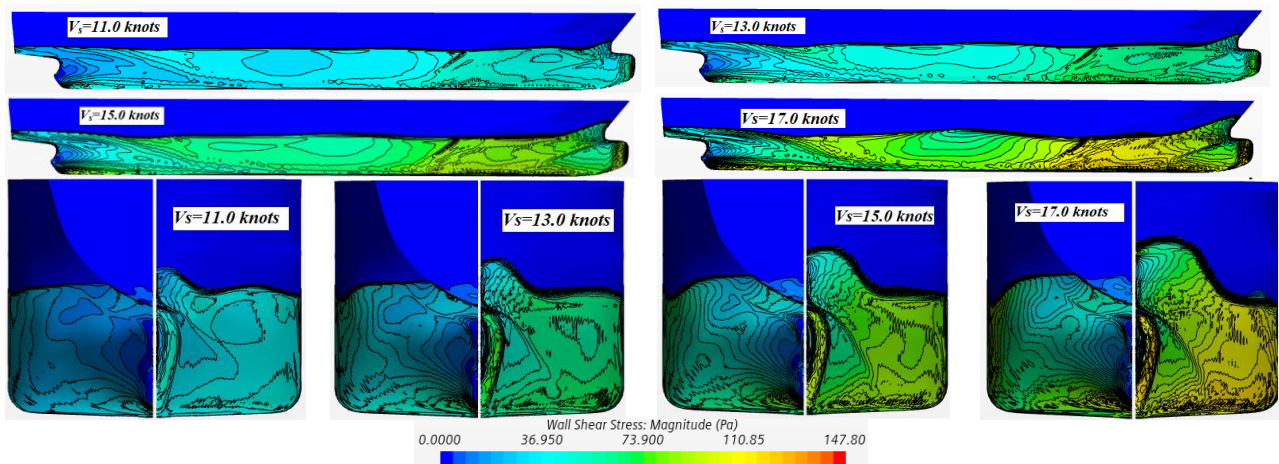
Fig. 11. Wall shear stress distribution on the containership hull surface at various ship speeds
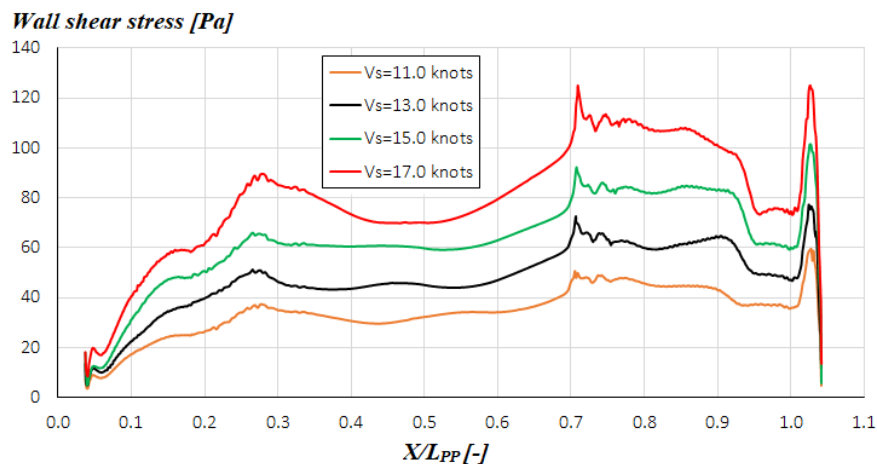
Fig. 12. Wall shear stress distribution at Z=4.0m with various ship speeds

An important hydrodynamic characteristic affecting the efficiency of the propeller located behind the ship is the nominal wake field at the propeller disc. Figure 13 presents the nominal wake field at the propeller disc at various ship speeds. As evident from the figure, the nominal wake field at the propeller disc is almost the same at various ship speeds.
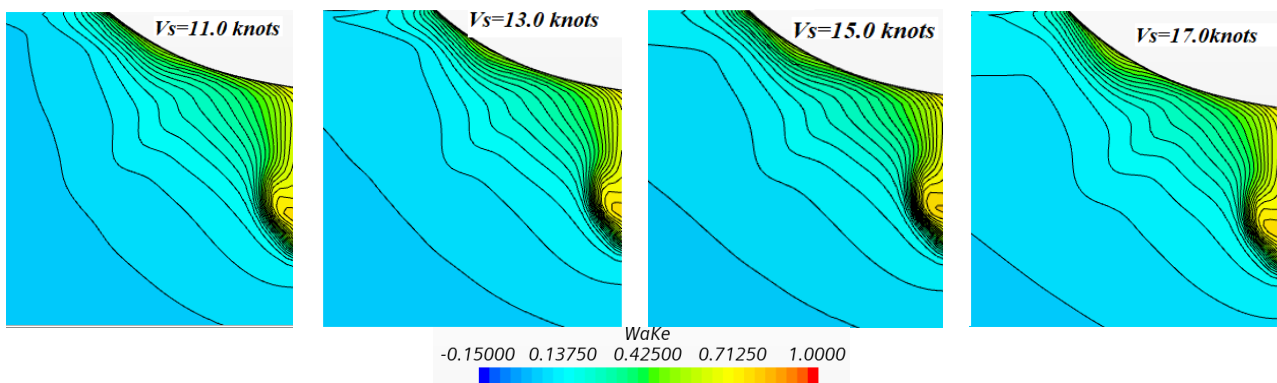
Fig. 13. Nominal wake on propeller disc at various ship speeds

5. Conclusions

This study successfully achieved its research objectives by employing the CFD method to predict the resistance and motions of the ship and simulating the flow patterns around the hull surface of containership at various speeds. The key findings from these simulations are detailed as follows

i. Predicted ship resistance and motions at design draught with different ship speeds in calm water conditions. The frictional and pressure resistance components have similar monotonically changing trend at different ship speeds, but different in level of change. Specifically, as ship speed increases, a larger increase is observed in the pressure resistance than in the frictional resistance. Trim and sinkage of the ship increase monotonically with increasing ship speed.

ii. The characteristics of wave pattern, volume fraction of air, distribution of dynamic pressure and wall shear stress coefficient on the hull surface, and the nominal flow field at the propeller disc at different ship speeds have been provided and analyzed. This could not only provide valuable insights into the change of ship resistance versus the ship speeds, but also is an important input data for the hull shape optimization in terms of minimizing ship resistance.

Acknowledgement

References

[1] Molland, Anthony F., Stephen R. Turnock, and Dominic A. Hudson. *Ship resistance and propulsion*. Cambridge University Press, 2017. https://doi.org/10.1017/9781316494196
[2] Kraskowski, Marek. "CFD optimisation of the longitudinal volume distribution of a ship's hull by constrained transformation of the sectional area curve." *Polish Maritime Research* 29, no. 3 (2022): 11-20. https://doi.org/10.2478/pomr-2022-0022
[3] Chuan, Tran Quoc, Nguyen Kim Phuong, Tran Ngoc Tu, Mai Van Quan, Nguyen Duy Anh, and Tat-Hien Le. "Numerical Study of Effect of Trim on Performance of 12500DWT Cargo Ship Using RANSE Method." *Polish Maritime Research* 29, no. 1 (2022): 3-12. https://doi.org/10.2478/pomr-2022-0001
[4] Choi, J. E., K-S. Min, J. H. Kim, S. B. Lee, and H. W. Seo. "Resistance and propulsion characteristics of various commercial ships based on CFD results." *Ocean Engineering* 37, no. 7 (2010): 549-566. https://doi.org/10.1016/j.oceaneng.2010.02.007
[5] Tu, T. N., N. T. H. Phuong, V. Tuan Anh, V. M. Ngoc, P. T. T. Hai, and C. H. Chinh. "Numerical prediction of ship resistance in calm water by using RANS method." *Journal of Engineering and Applied Sciences* 13, no. 17 (2018): 7210-7214.
[6] Haase, Max, Konrad Zurcher, Gary Davidson, Jonathan R. Binns, Giles Thomas, and Neil Bose. "Novel CFD-based full-scale resistance prediction for large medium-speed catamarans." *Ocean Engineering* 111 (2016): 198-208. https://doi.org/10.1016/j.oceaneng.2015.10.018
[7] Nasirudin, Ahmad, I. Ketut Aria Pria Utama, Sutiyo Sutiyo, and Andreas Kukuh Priyasambada. "CFD Analysis into the Resistance Estimation of Hard-Chine Monohull using Conventional against Inverted Bows." *CFD Letters* 15, no. 6 (2023): 54-64. https://doi.org/10.37934/cfdl.15.6.5464
[8] Ahmed, Alaaeldeen Mohamed Elhadad. "Comparative investigation of resistance prediction for surface combatant ship model using CFD modeling." *Journal of Advanced Research in Fluid Mechanics and Thermal Sciences* 107, no. 2 (2023): 225-235. https://doi.org/10.37934/arfmts.107.2.225235
[9] Ahmed, Alaaeldeen Mohamed Elhadad, and Ahmed Mokhtar Abo El-Ela. "Experimental and CFD Resistance Validation of Naval Combatant DTMB 5415-51 Model." *Journal of Advanced Research in Fluid Mechanics and Thermal Sciences* 107, no. 2 (2023): 84-102. https://doi.org/10.37934/arfmts.107.2.84102
[10] Hänninen, Satu, and Juha Sehweighofer. "Numerical investigation of the scale effect on the flow around a ship hull." *Ship Technology Research* 53, no. 1 (2006): 17-25. https://doi.org/10.1179/str.2006.53.1.004
[11] Song, Ke-wei, Chun-yu Guo, Chao Wang, Cong Sun, Ping Li, and Ruo-fan Zhong. "Experimental and numerical study on the scale effect of stern flap on ship resistance and flow field." *Ships and Offshore Structures* 15, no. 9 (2020): 981-997. https://doi.org/10.1080/17445302.2019.1697091
[12] Le, Tat-Hien, Nguyen Duy Anh, Tran Ngoc Tu, Nguyen Thi Ngoc Hoa, and Vu Minh Ngoc. "Numerical investigation of length to beam ratio effects on ship resistance using RANSE method." *Polish Maritime Research* 30, no. 1 (2023): 13-24. https://doi.org/10.2478/pomr-2023-0002
[13] Le, Tat Hien, and Tran Van Tao. "Numerical Investigation of the Scale Effect on the Flow around the Ship by using RANSE Method." *CFD Letters* 15, no. 11 (2023): 67-78. https://doi.org/10.37934/cfdl.15.11.6778
[14] Hoa, Nguyen Thi. "Numerical Prediction of Ship's Self-Propulsion Parameter by Using CFD Method." *TransNav, the International Journal on Marine Navigation and Safety of Sea Transportation* 18, no. 2 (2024). https://doi.org/10.12716/1001.18.02.22
[15] Tu, Tran Ngoc, Vu Minh Ngoc, Nguyen Thi Thu Quynh, Nguyen Manh Chien, Nguyen Thi Hai Ha, and Nguyen Thi Ha Phuong. "Effects of Turbulence Models On RANSE Computation Of Flow Around DTMB 5415 Vessel." *Naval Engineers Journal* 133, no. 3 (2021): 137-151.
[16] Le, Tat-Hien, Mai The Vu, Vu Ngoc Bich, Nguyen Kim Phuong, Nguyen Thi Hai Ha, Tran Quoc Chuan, and Tran Ngoc Tu. "Numerical investigation on the effect of trim on ship resistance by RANSE method." *Applied Ocean Research* 111 (2021): 102642. https://doi.org/10.1016/j.apor.2021.102642
[17] Siemens. *STAR-CCM+ User Guide. Version 16.4*. Siemens, 2021.
[18] Abobaker, Mostafa, Sogair Addeep, Lukmon O. Afolabi, and Abdulhafid M. Elfaghi. "Effect of mesh type on numerical computation of aerodynamic coefficients of NACA 0012 airfoil." *Journal of Advanced Research in Fluid Mechanics and Thermal Sciences* 87, no. 3 (2021): 31-39. https://doi.org/10.37934/arfmts.87.3.3139

[19]   ITTC. "ITTC - Recommended Procedures and Guidelines. Practical Guidelines for Ship Re sistance CFD." *International Towing Tank Conference*, 2014. https://ittc.info/media/4198/75-03-02-04.pdf.

[20]   Larsson, Lars, Hoyte C. Raven, and J. Randolph Paulling. "Ship resistance and flow." *Published by The Society of Naval Architects and Marine Engineers, SNAME, The Principles of Naval Architecture Series, ISBN: 978-0-939773-76-3* (2010).